NMRF/RR/06/2024

RESEARCH REPORT

Study of Indian Ocean features during 2023 summer monsoon using NCMRWF coupled model

Lokesh Pandey, Ankur Gupta, and Akhilesh K. Mishra

May 2024

National Centre for Medium Range Weather Forecasting
Ministry of Earth Sciences, Government of India
A-50, Sector 62, Noida-201309, INDIA

Study of Indian Ocean features during 2023 summer monsoon using NCMRWF coupled model

Lokesh Pandey, Ankur Gupta, and Akhilesh K. Mishra

NMRF/RR/06/2024

National Centre for Medium Range Weather Forecasting

Ministry of Earth Sciences

A-50, Sector 62, Noida-201309, INDIA

www.ncmrwf.gov.in

Ministry of Earth Sciences

National Centre for Medium Range Weather Forecasting

Document Control Data Sheet

1	Name of the Institute	National Centre for Medium Range Weather Forecasting
2	Document Number	NMRF/RR/06/2024
3	Date of publication	May 2024
4	Title of the document	Study of Indian Ocean features during 2023 summer monsoon using NCMRWF coupled model
5	Type of Document	Research Report
6	No.of pages & Figures	42 pages including 16 figures
7	Number of References	75
8	Author (S)	Lokesh Pandey, Ankur Gupta, and Akhilesh K. Mishra
9	Originating Unit	NCMRWF
10	Abstract	Indian Ocean plays an important role in determining the variability of monsoon rainfall at different time scales. With the development of ocean data assimilation system and improvement in representation of air-sea interaction in the dynamical models, prediction of ocean-atmosphere state at extended leadtime has been made possible. An extended range prediction system is running in real-time at NCMRWF. In this study, thermodynamical ocean features during June-September (JJAS) 2023 have been studied using both observations and model forecast. The ability of the model in representing the large scale spatial pattern of key ocean variables has been assessed. Comparison of weekly-mean and month-mean ocean variables is carried out against model analysis and observations. It is found that model captures well the spatial patterns of SST, SSS, SSH, D20, MLD, and upper ocean heat content. However, systematic biases in upper ocean variables have been found which are seen to increase with leadtimes. The east-west contrast in SST, SSH, and thermocline shows the importance of equatorial processes such as upwelling in simulation of upper ocean thermodynamical

		variables.
11	Security classification	Non-Secure
12	Distribution	Unrestricted Distribution
13	Keywords	Indian Ocean, Extended Range Forecasts, Seamless modelling, Coupled Model

Table of Contents

Study of Indian Ocean features during 2023 summer monsoon using NCMRWF coupled model

Lokesh Pandey, Ankur Gupta, and Akhilesh K. Mishra

सारांश

हिंद महासागर अलग-अलग समय के पैमाने पर मानसूनी वर्षा की परिवर्तनशीलता को निर्धारित करने में महत्वपूर्ण भूमिका निभाता है। महासागर डेटा आत्मसात प्रणाली के विकास और गतिशील मॉडल में वायुमंडल-समुद्र संपर्क के प्रतिनिधित्व में सुधार के साथ , विस्तारित लीडटाइम पर महासागर-वायुमंडल की स्थिति की भविष्यवाणी संभव हो गई है। एन॰सी॰एम॰आर॰डब्ल्यू॰एफ॰ में एक विस्तारित रेंज पूर्वानुमान प्रणाली वास्तविक समय में चल रही है। इस शोध लेख में, महासागर की वास्तविक स्थिति और मोडेल के पूर्वानुमान का उपयोग करके 2023 जे॰जे॰ए॰एस॰ के दौरान महासागर की थर्मोडायनामिकल विशेषताओं का अध्ययन किया गया है। प्रमुख महासागरीय चरों के बड़े पैमाने पर स्थानिक पैटर्न का प्रतिनिधित्व करने में मॉडल की क्षमता का आकलन किया गया है। यहाँ मुख्य समुद्री विशेषताओं के साप्ताहिक-माध्य और माह-माध्य संयोजन की गणना की गयी है और इनकी तुलना मॉडल विश्लेषण और ऑब्जरवेशन के साथ की गयी है। यह पाया गया है कि मॉडल एसएसटी, एसएसएस, एसएसएच, डी20, एमएलडी और ऊपरी समुद्री ताप सामग्री के स्थानिक पैटर्न को अच्छी तरह से पकड़ लेता है। हालाँकि, ऊपरी महासागरीय चरों में व्यवस्थित पूर्वाग्रह पाए गए हैं जिन्हें लीडटाइम के साथ बढ़ते देखा गया है। एसएसटी, एसएसएच और थर्मोकलाइन में पूर्व-पश्चिम कंट्रास्ट का होना, ऊपरी महासागर थर्मोडायनामिकल चर के अनुकरण में उत्थान जैसी भूमध्यरेखीय प्रक्रियाओं के महत्व को दर्शाता है।

Abstract

Indian Ocean plays an important role in determining the variability of monsoon rainfall at different time scales. With the development of ocean data assimilation system and improvement in representation of air-sea interaction in the dynamical models, prediction of ocean-atmosphere state at extended leadtime has been made possible. An extended range prediction system is running in real-time at NCMRWF. In this study, thermodynamical ocean features during June-September (JJAS) 2023 have been studied using both observations and model forecast. The

ability of the model in representing the large scale spatial pattern of key ocean variables has been assessed. Comparison of weekly-mean and month-mean ocean variables is carried out against model analysis and observations. It is found that model captures well the spatial patterns of SST, SSS, SSH, D20, MLD, and upper ocean heat content. However, systematic biases in upper ocean variables have been found which are seen to increase with leadtimes. The east-west contrast in SST, SSH, and thermocline shows the importance of equatorial processes such as upwelling in simulation of upper ocean thermodynamical variables.

1 Introduction

The coupled atmosphere-ocean processes are important for Indian Summer Monsoon (ISM) Rainfall (ISMR). Timely and accurate prediction of ISMR is crucial for management of water resource, agricultural practices and several others aspects of the Indian economy (Dwivedi et al., 2006, 2015; S Gadgil & Gadgil, 2006). The formation and variability of the Asian monsoon system is influenced greatly by the air-sea interactions in the Indian Ocean (IO) (Gadgil, 2003; Gadgil et al., 2005; Webster et al., 1998). For example, the variability of the sea surface temperatures (SST) in the Indian Ocean directly influences the predictability and prediction of the ISMR on different time scales (Mishra et al., 2020; Rajeevan et al., 2007, 2012; Sahai et al., 200 C.E.; Yang et al., 2007). The IO region experiences large changes in the direction and magnitude of winds from southwesterly during summer to northeasterly during winter. The upper ocean circulation in the IO also shows strong seasonality and experiences complete reversal of direction of major ocean currents in the region (F. A. Schott et al., 2009). The weather and climate in others parts of the world are also significantly influenced by the IO. The ocean regulates the transfer of heat to the atmosphere through surface heat fluxes by acting as a heat reservoir. Therefore, it is crucial to incorporate the ocean as an essential component in dynamical modeling systems.

Prediction of the Indian monsoon is a challenging task. Studies shows several deficiencies in the simulation of the ISMR in the climate models which can impact the skill in predicting the monsoons (Anand et al., 2018; Saha et al., 2014; Wang et al., 2015). The errors in simulating the monsoons can come from difficulties in parameterization of convective processes in the dynamical models. In addition, lack of sufficient high-resolution (eddy resolving) initial

conditions for the IO can also contribute to errors in simulating the ISMR (Goswami et al., 2016; Koul et al., 2018; Rao et al., 2019). To generate the best estimates of ocean initial condition, dense and continuous in time quality-controlled in-situ observations in the IO need to be collected via sea cruises, Argo floats, moorings, gliders etc (Davis et al., 2018; Subramanian et al., 2019). The accurate initial conditions and forcings of Arabian Sea (AS) and Bay of Bengal (BOB) are crucial for correctly simulating the onset and propagation of ISMR during the monsoon season (Goswami et al., 2016; Rao & Sivakumar, 1999; Shenoi et al., 1999). It is not possible for the sea-going oceanographers to collect quality-controlled in situ (depth dependent) observations at all grid points in the northern Indian Ocean with the help of observational campaigns. This leaves the in-situ observations with limited spatio-temporal coverage. The modern satellite measurements on the other hand have very good space-time coverage, but they are restricted to surface variables only. The recourse is taken by carrying out ocean modeling at desired spatio-temporal resolution to generate 3-dimensional continuous in time initial conditions and forcings of the northern IO.

The development of ocean data assimilation systems and improvements in representation of coupled processes has improved the representation of air-sea interactions and intraseasonal variability in dynamical models (Belcher et al., 2015; Klingaman & Woolnough, 2014). These improvements has resulted in extending the skill of numerical weather systems to 2-3 weeks for low frequency variability of the tropical atmosphere (Abhilash et al., 2014). Recently, there has been interest in the extended range prediction of ocean variables as well. An extended range prediction system is also running at National Center for Medium Range Weather Forecasting (NCMRWF) as part of the seamless modeling strategy. Gera et al., 2022 have shown the model

is skillful in predicting the active and break phases of the monsoons up to two weeks in advance. However, the performance of the model in simulating the ocean features is not known.

This report documents the performance evaluation of the global NCMRWF coupled NCMRWF Unified Model (CNCUM) forecasts during JJAS 2023. The primary objective of this study is to assess the ability of the model in capturing the key thermodynamic features of the IO. The large scale patterns of SST, salinity, mixed layer depth (MLD) etc during the 2023 monsoon season and the processes governing these spatial distribution are highlighted first. The model simulations are presented next and compared with model analyses and observations. The results are summarized through careful verification, shining light on the average biases and forecast performances for the entire season. Section 2 describes the coupled model used in this study, the data processing methodology adopted for computing the composites, and the model analyses used for initializing the model, and observational datasets utilized for comparing forecasts. Sections 3 to 5 of the report investigate the systematic biases found in the forecasted large-scale upper ocean fields, encompassing crucial elements such as temperature, salinity, MLD and Sea Surface Height among others. The insights provided in these sections prove to be invaluable in enabling forecasters to interpret the model forecasts more effectively and make informed decisions. Finally, Section 7 serves as a comprehensive culmination of the JJAS 2023 report. It succinctly summarizes the key findings, strengths, and limitations of the CNCUM model forecasts of ocean variables during this monsoon season. The summary offers valuable takeaways for both forecasters and model developers, aiding them in refining the forecasting process and enhancing the model's performance in subsequent seasons.

2 Data and Methodology

The coupled model used in this incorporates the Unified Model (UM) to represent the atmospheric component and the Joint United Kingdom Land Environment Simulator (JULES) model to represent the land component. The land-atmosphere model is coupled to an ocean-seaice model. Nucleus European Modeling of Ocean (NEMO: Madec, 2008) forms the ocean component of the ocean-seaice model and Los Alamos seaice model (CICE) represents the thermodynamics and elastic-viscous-plastic processes of the seaice (Hunke & Dukowicz, 1997). The coupling between the component models is achieved using version 3.0 of OASIS (Valcke, 2013).

The land-atmosphere model is defined on an N216 grid, where N implies 1.5xN and 2xN grid points in meridional and zonal direction, respectively. The atmospheric model extends up to 85 km in vertical which cover the stratosphere, and the vertical extent is divided into 85 levels, 50 of which are in troposphere (below 18 km). The horizontal discretization uses Arakawa C-grid staggering, while vertical discretization follows Charney-Phillips staggering. The ocean-seaice model is defined on an eddy-permitting ¼◦ tripolar orthogonal curvilinear grid with two poles respectively at 107◦W and 73 ◦E in Siberia and Canada. The importance of resolving eddies on atmospheric variability has been shown in a large number of studies on western boundary currents (Kelly et al., 2010; Ma et al., 2017). Arakawa C-grid staggering is used for the horizontal discretization, except prognostic variables in CICE are defined on Arakawa B-grid. The model has high vertical resolution especially near the surface. The 75-level z-coordinate has vertical resolution of 1 m near the surface and increasing to 200 m at 6000 m. The DRAKKAR v3.3 bathymetry used here is an update from a 1-minute resolution ETOPO1 data set (Amante & Eakins, 2009) with additional information in coastal regions from GEBCO (IOC & In, 2003).

The science configuration is based on Global Coupled version 2.0 (GC2) and is completely described in (Williams et al., 2015). The GC2 is the first science configuration adopted by an operational center to be used for forecasting across the time scales. Semi-implicit semi-Lagrangian formulation is used for solving the non-hydrostatic, fully compressible deep-atmosphere. Atmospheric physical processes such as convection, boundary layer turbulence, cloud formation, radiation, orographic drag, etc. are parameterized in the model. Further details can be seen in Gupta et al., 2019 and Williams et al., 2015. Ocean model solves a vector invariant form of prognostic equations in which an enstrophy and kinetic energy conserving scheme is used to discretize vorticity. The model is integrated in time using the leapfrog time-differencing scheme of Mesinger & Arakawa, 1976. Oceanic processes such as diapycnal mixing, energy transfer due to internal tides breaking, diffusion both in interior and boundary layer are parameterized. Detailed scientific configurations for individual component are defined by Walters et al., 2017 for land-atmosphere, Megann et al., 2014 for ocean, and Rae et al., 2015 for seaice.

The coupled model in the NCMRWF extended range prediction (NERP) system is initialized four days in a week from separate analyses of land-atmosphere and ocean–seaice components. The model is initialized on Sunday to Wednesday of each week; the simulation length for each initialized model is 36 days. The analysis for initializing the coupled model comes from real-time NCMRWF ocean and atmosphere data assimilation systems. The atmospheric data assimilation system uses both conventional and satellite data in a 4-D variational assimilation scheme (George et al., 2016; Kumar et al., 2020). The surface temperature, salinity and temperature profiles, and sea level anomalies are assimilated in a 3D-VAR ocean data

assimilation system with First Guess at Appropriate Time (FGAT) approach(Momin et al., 2020; Waters et al., 2015).

In the NERP system the coupled model is initialized on Sunday to Wednesday of each week. Each week, forecasts are prepared on Thursday using the data from model initialized on Sunday, Monday, Tuesday and Wednesday immediately preceding the day forecasts are prepared. The daily ensemble-mean forecasts falling on Friday to Thursday are then combined into weekly averages. Week-1 forecast is prepared from the data valid from days 1 to 7 following each Thursday. Similarly, week-2, week-3, and week-4 forecasts are prepared from data valid on 8-14, 15-21, 22-28 days following each Thursday, respectively. All the forecasts having the data valid from JJAS 2023 are then combined to make composites of week-1 to week-4 forecasts. To analyze the performance of the model, weekly-averaged observations and model-analysis are prepared using the same method as of model forecasts. While analyzing monthly-mean forecasts, forecasts prepared on the last Thursday of the month preceding the validity month are considered.

For validating model simulations for SST, National Oceanic and Atmospheric Administration (NOAA) daily Optimum Interpolation SST SSTv2.1 (Reynolds et al., 2007) data at 0.25^0 resolution is used. Forecasts of other variables are compared with model's own analysis.

Ocean Heat Content (OHC) is a significant climatic factor within the ocean-atmosphere system, playing a crucial role in determining heat exchange dynamics. Its impact extends to weather phenomena such as cyclones and monsoons. Therefore, an accurate assessment of OHC is crucial for comprehending the oceans' role in evaluating historical and projected climate change. Heat content of a slice of the ocean can be estimated as a product of integrated temperature,

density of sea water and specific heat capacity from surface down to a required depth. It is obtained by summing the heat content of the ocean column from the sea surface to a particular depth. OHC can be computed from the equation given below:

$OHC = C_p \int_0^D \rho(z) T(z) dz$ where ρ is the density of seawater computed using temperature and salinity, cp (4000 J/Kg/K) is the specific heat capacity of seawater, T(z) is the temperature as a function of depth (z), D is the depth of the ocean. Here D = 300 m. Similarly, MLD are computed using a density criteria, i.e. the depth at which density is higher than that at surface corresponding to a 0.8°C decrease in temperature (Kara et al., 2000). The variations in depth of thermoclines are studies by analyzing the depth of 20 ^{o}C isotherm (D20).

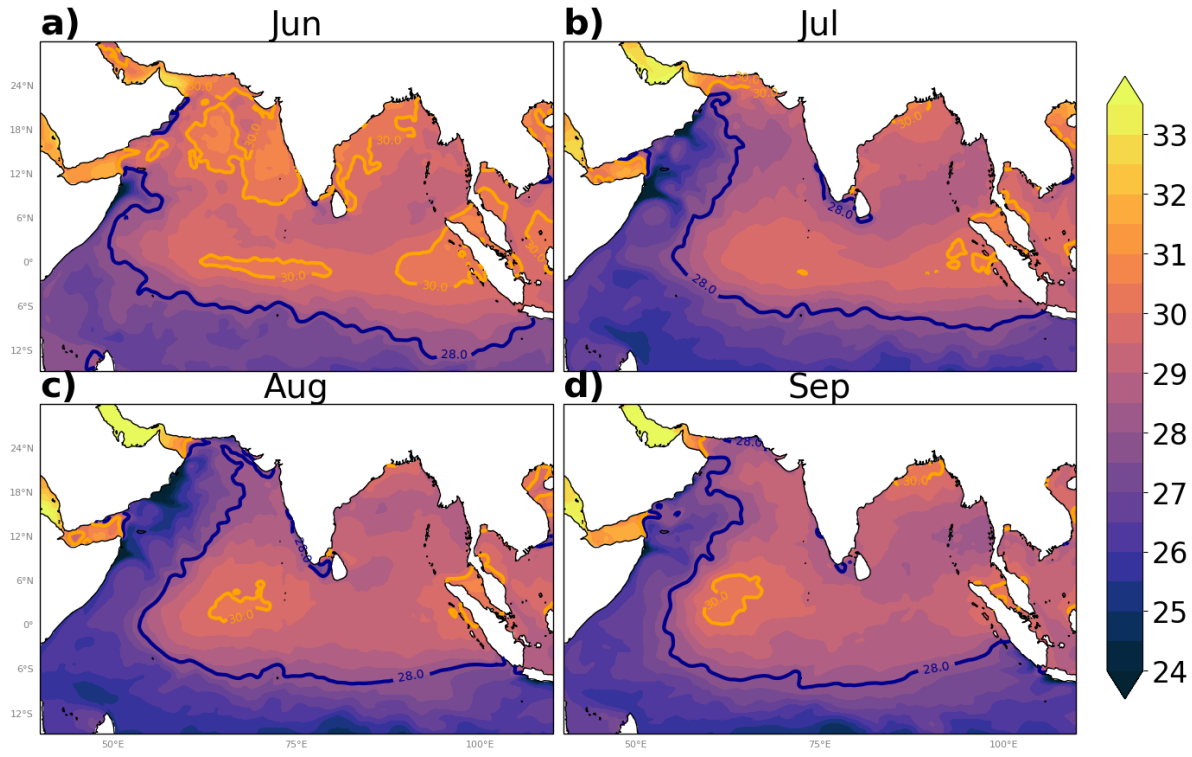

Figure 1 Observed SST pattern (shaded) during 2023 a) June, b) July, c) August, and d) September. SST above 28 ^{o}C and 30 ^{o}C are highlighted using blue and yellow contours, respectively.

3 Observed Features during 2023 JJAS

As discussed above, SST is one of the most important parameter affecting the air-sea interaction and thus the convection. Thus, we begin the analysis of 2023 summer season by showing the spatial patterns of SST during each month of JJAS in Figure 1. It can be seen that very warm waters are present in the north IO particularly during the month of June. It is interesting to note that during June much of the AS and part of BOB experienced waters even above 30^{o}C. While it is known that the IO is warming at an unprecedented rate (Rao et al., 2012; Roxy et al., 2014) the extent of pool of water above 28^{o}C usually decreases substantially by the September (Vinayachandran & Shetye, 1991). However, in 2023 there is little change in the extent of the warm pool. The entire north IO with the exception of the western AS remained above 28 ^{o}C – a threshold generally considered to be favorable for convection (Gadgil et al., 1984). The warming of the IO during 2023 is an interesting case – being an El-Nino year accompanied by a late monsoon onset (8th June). Warmest waters towards the end of the monsoon season appear over the equator from 60-70^{o}E.

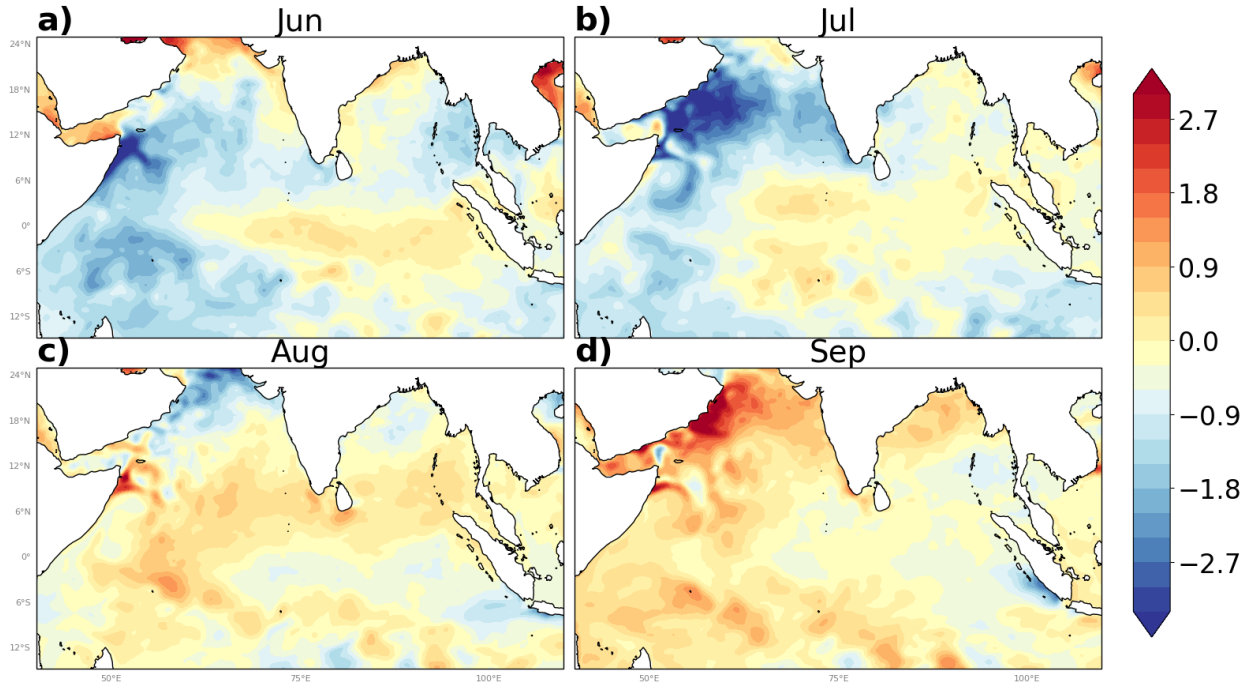

Figure 2 Changes in SST (^{o}C) during a) June, b) July, c) August, and d) September of 2023 with respect to the previous month.

The SST in the IO are largely driven by surface fluxes. The unique interaction of the monsoon winds with the subsurface thermal structure of the ocean determines the intra-seasonal changes

of SST. The tendencies of SST in each of the month of JJAS are shown in Figure 2. It can be seen that most of the cooling is seen in the AS along the coasts of Somali and the Arabian Peninsula during the months of June and July and over the north AS during August. Interestingly, the cooling during the monsoon over the AS quickly gives way to the warming in September, most-intense along the coast of the Arabian Peninsula. Similar changes but of much milder intensity are seen over the BOB which most notably experience warming in September. The WEIO also experiences similar reversal in nature of SST changes within the season: beginning the season with cooling in June-July and switching to warming in August-September. Perhaps the most interesting is the SEEIO; it shows mild warming throughout the season except for large cooling in September which is restricted to waters along the Sumatra coast.

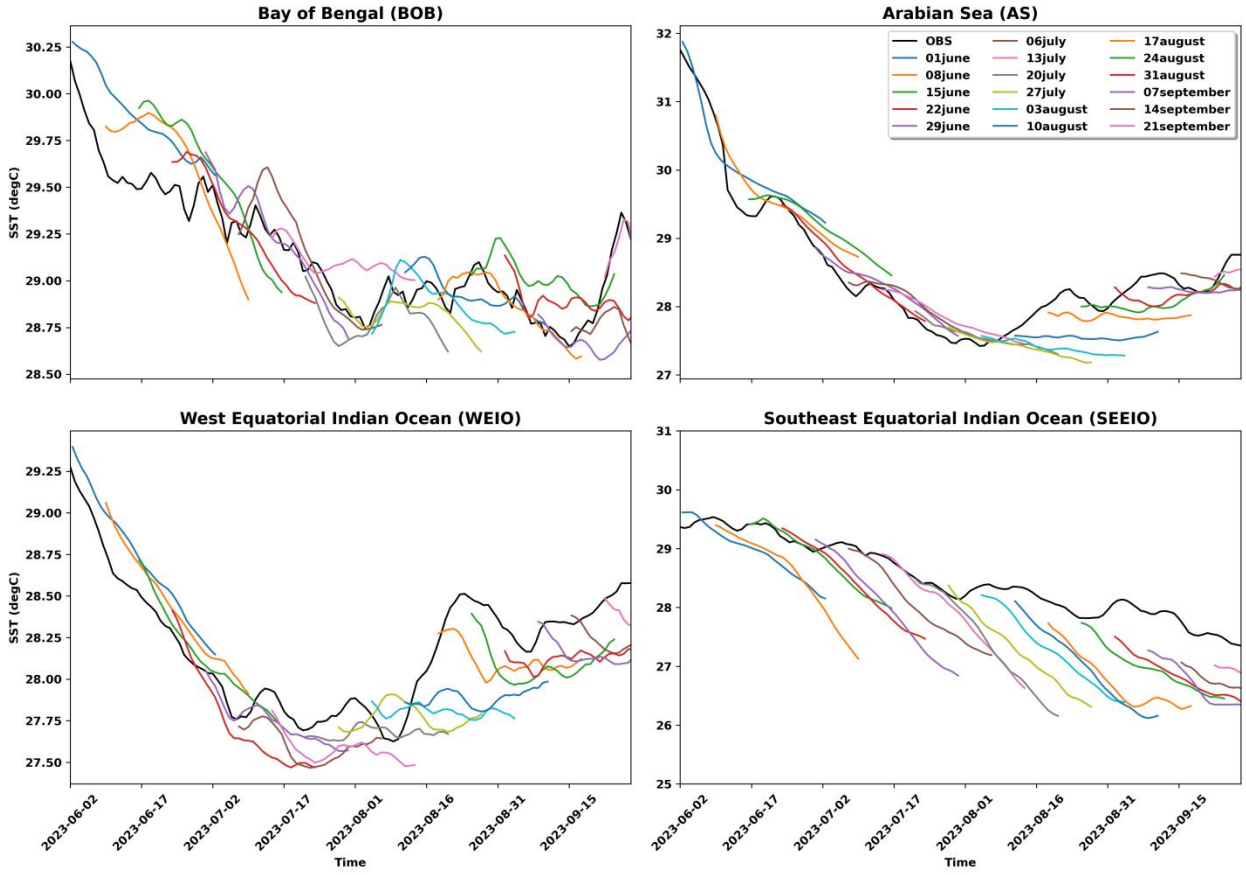

Figure 3 Average SST over the different regions of Indian ocean (a): Bay of Bengal (BOB:10–18 N, 85–93 E), (b): the Arabian Sea (AS: 10–18 N, 60–70E), (c): the west equatorial Indian Ocean (WEIO: 10S-10 N, 50–70E), and (d): the southeast equatorial Indian Ocean (SEEIO 10S-0, 90–110E) from observations and the different initial conditions during JJAS for a period of 36 days each. Black bold line is the observation from NOAA OI SST (Reynolds et.al 2007).

In Figure 3 the area averaged SST over different regions of the Indian Ocean is presented which brings out the intraseasonal changes in the SST more clearly. These regions are: Bay of Bengal (BOB:10–18 N, 85–93 E), the Arabian Sea (AS: 10–18 N, 60–70E), the west equatorial Indian Ocean (WEIO: 10S-10 N, 50–70E), and the southeast equatorial Indian Ocean (SEEIO 10S-0, 90–110E). The observed SST data are from the optimum interpolation of in-situ and bias-corrected satellite-derived observations Reynolds et al., 2007. Before discussing the weekly-mean model forecasts we briefly present the performance of model in capturing this seasonal cycle. Thus, in Figure 3 the model forecasts (colored lines) of area-averaged SST at up to 36-days of leadtimes are also overlaid over observed SST (black lines) for all forecasts initialized during JJAS. As discussed earlier both AS and BOB shows cooling during the June-July and warming in September. These changes are likely mediated by the monsoonal winds. At the beginning of the season both AS and BOB shows peak SST. These early warm SST are in response to pre-monsoon insolation over clear skies augmented by lack of poleward (northward) advection of heat, the ocean being bounded to the north by the Indian landmass. With the onset of the monsoon on 8th June 2023, the monsoonal winds quickly cool the upper ocean by as much as 4 ^{o}C in the AS but only 1 ^{o}C in the BOB. This difference in response of AS and BOB is widely documented (Prasad, 2004; Shenoi et al., 2002). The monsoon winds have higher intensity over the AS compared to BOB. However, the waters are highly stratified in the BOB which prevents the relatively weaker winds over the bay to mix the surface waters with the cold waters underneath. This means that while the energy available for mixing the waters is high in the AS, the energy required for mixing is high in the BOB due to which the bay shows resistance to large winds driven changes in the SST (Shenoi et al., 2002). Second to the seasonal cycle, large intraseasonal variations in SST can also be seen in Figure 3.

It is seen from the plot that the model brings out reasonably well the seasonal cycle of the JJAS of the southwest monsoon season (JJAS). The representation of SST in the model for JJAS is captured for all the regions (Figure 3 a-c) except southeast equatorial Indian Ocean. At the beginning of the season the model initial SST over SEEIO are close to the observations; however, during September even the model initial estimates of the SST are far off from the observations. The model's inability in capturing the SST over the SEEIO region even at the start of the simulation could be due to lack of in-situ data to constraint the model-analysis, biases in forcing the ocean during data assimilation stages, as well as difficulties in assimilating both in-

situ and satellite data over the region. Nevertheless, the drift of simulated SST over SEEIO increases fast with the leadtimes irrespective of the startdate. This could suggest model's inability in capturing the mixed layer processes over the SEEIO. Gupta et al., 2022 shows that such biases in the coupled models could also result from errors in simulation of equatorial winds.

It can be seen that model reproduction of SST in the AS is remarkably good during June-July. Similarly, the cooling of SST in the BOB and WEIO during June-July is captured by the model. However, model shows cold bias over AS and WEIO as well during August-September similar to SEEIO.

4 Weekly-mean Forecasts

In this section week-1, week-2, week-3, and week-4 forecasts of key ocean variables are shown. Comparison of forecasts is done with observations and model-analysis.

4.1 Sea Surface Temperature

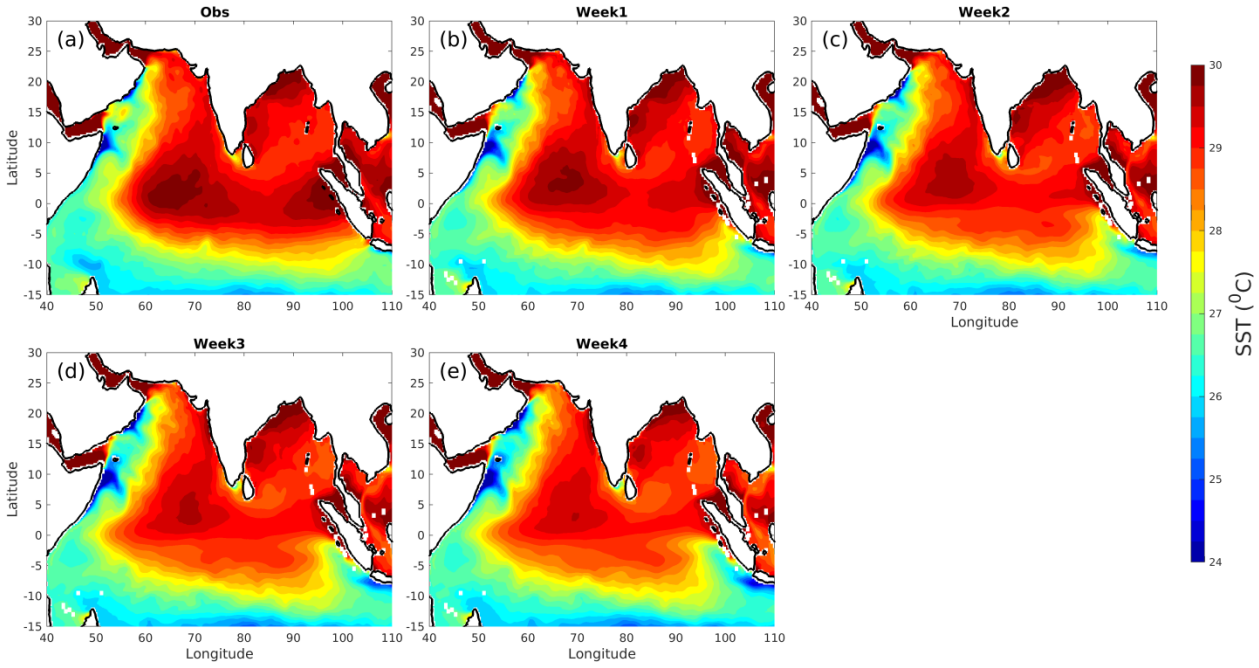

Figure 4 Mean SST (^{0}C) during JJAS. (a) observations for dates falling within week-1 of model initialization. Week-1, week-2, week-3, and week-4 forecasts are shown in b), c), d), and e) respectively.

Figure 4a shows observed SST during JJAS 2023 . Week-1, week-2, week-3, and week-4 forecasts from CNCUM are also shown in Figure 4b-e.. Three main regions of warm ocean waters are seen in the observations: the head BOB, WEIO, and SEEIO. Significantly warmer waters are present over the BOB as compare to AS. As discussed above, while the SST are higher in June over both AS and BOB, the cooling over BOB is much smaller compared to AS. This results in warmer SST over BOB compared to AS. Within the bay warmest waters are flanked to the north, a region near to the mouth of the Ganga-Brahmaputra river system. This may result in salt stratification of the bay inhibiting the vertical mixing. Indeed, the shallowest MLD in the region are also observed over the head BOB. Temperatures are relatively cooler over the WEEIO and along the coasts of Somali and the Arabian Peninsula which are one of the key areas of upwelling cold underneath water in the north Indian Ocean. Somalia-Oman upwelling is caused by southeastward offshore Ekman ocean transport along the strong low-level southwesterly jet in atmosphere (De Boyer Montégut et al., 2007; Findlater, 1969). The variability of cooling associated with the jet can significantly affects the ISM (Izumo et al., 2008). In 2023, a strong cooling is observed in June along the Somali Coast which spreads towards the coast of Arabian Peninsula and also in the interior of the AS (Figure 2). This results in low SST along the western coast of AS.

It can be seen that model captures the spatial distribution of regions of warm and cold SST remarkably well even in week-4 forecast. However, some key deviations from the observations can be seen (Figure 4 b-e). It has been observed that week-1 forecast of SST magnitude agrees well with the observation. For week-2 to week-4 forecasts, slight cooling is seen in the model compared to observations. The peak of SST along the coast of Sumatra is much weaker in model

simulations even in week-1 forecasts, and by week-4 the peak of SST over SEEIO is completely absent in the model. Nevertheless, warm head BOB, peak of SST over WEIO, and cold southern IO and cold west coast of AS are well represented in week-1 to week-4 forecasts.

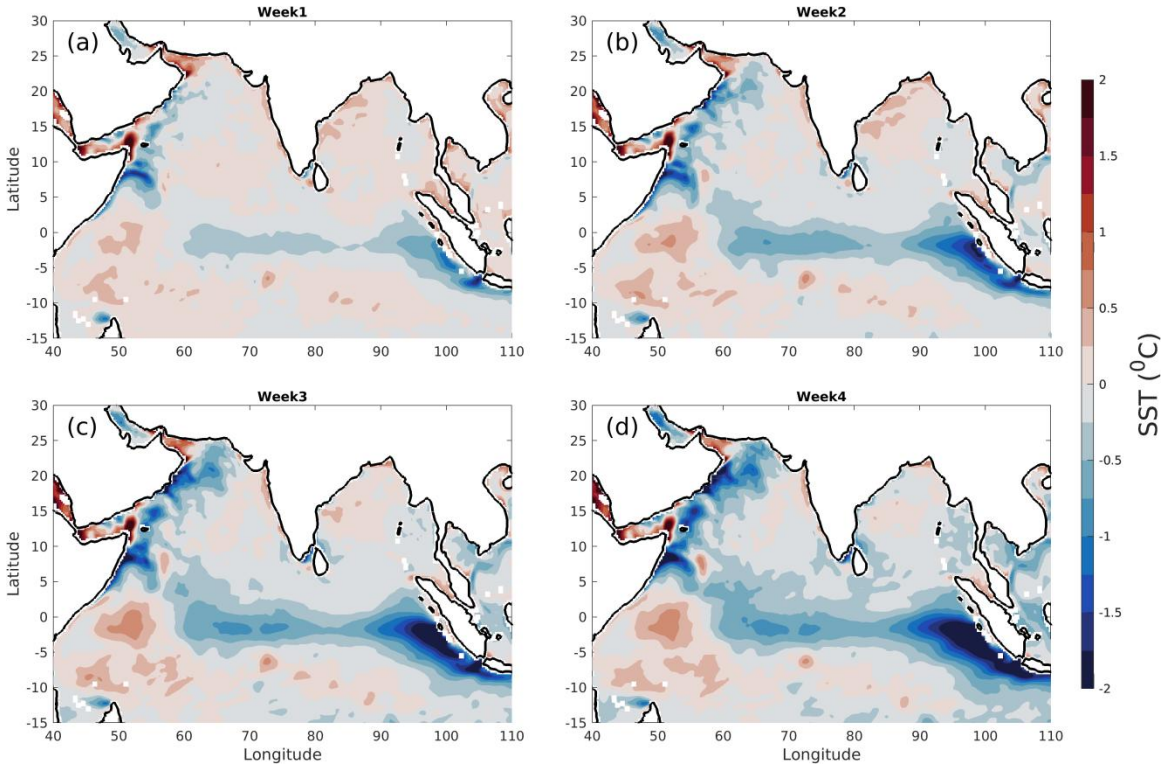

Figure 5 SST biases for (a) week-1, (b) week-2, (c) week-3 and (d) week-4 forecast

To further study the growth of errors in SST simulations from week-1 to week-4, the biases valid over different weeks are shown in Figure 5. The biases are computed by subtracting the week-1, week-2, week-3 and week-4 composites of observations from corresponding model composites using the methodology described in section 2. It can be seen from Figure 5 that the coupled model shows cold biases over the Somali Jet region, central equatorial IO and SEEIO. These biases could be related to excessive wind intensity in the model (Gupta et al., 2022). The cold biases during JJAS in the AS are limited towards the upwelling regions of Somali Jet suggesting the role of upwelling favorable winds during JJAS. Similarly, the cold biases over SEEIO are also located over an upwelling sensitive region. The biases over SEEIO warrants further study,

as the area is one of key region in a developing Indian Ocean dipole (Saji et al., 1999). Studies indicate that the SST in the region is an outcome of the balancing effects of warm water advection by the Indonesian Throughflow (ITF) and cooling by upwelling-favorable winds during and after boreal summer (Du et al., 2008).

In contrast, a warm bias is present over WEIO. Here the warm biases could be related to weaker winds in the model compared to observations (Gupta et al., 2022) and also due to downwelling Rossby waves travelling in response to coupled processes in the eastern part of the equatorial Indian Ocean. In all of the weeks, the spatial pattern of the biases remains similar with some areas showing much larger growth in biases with lead times. It can be seen from Figure 5 that the week-1 biases are less than + /- 0.5 ◦C in most areas.

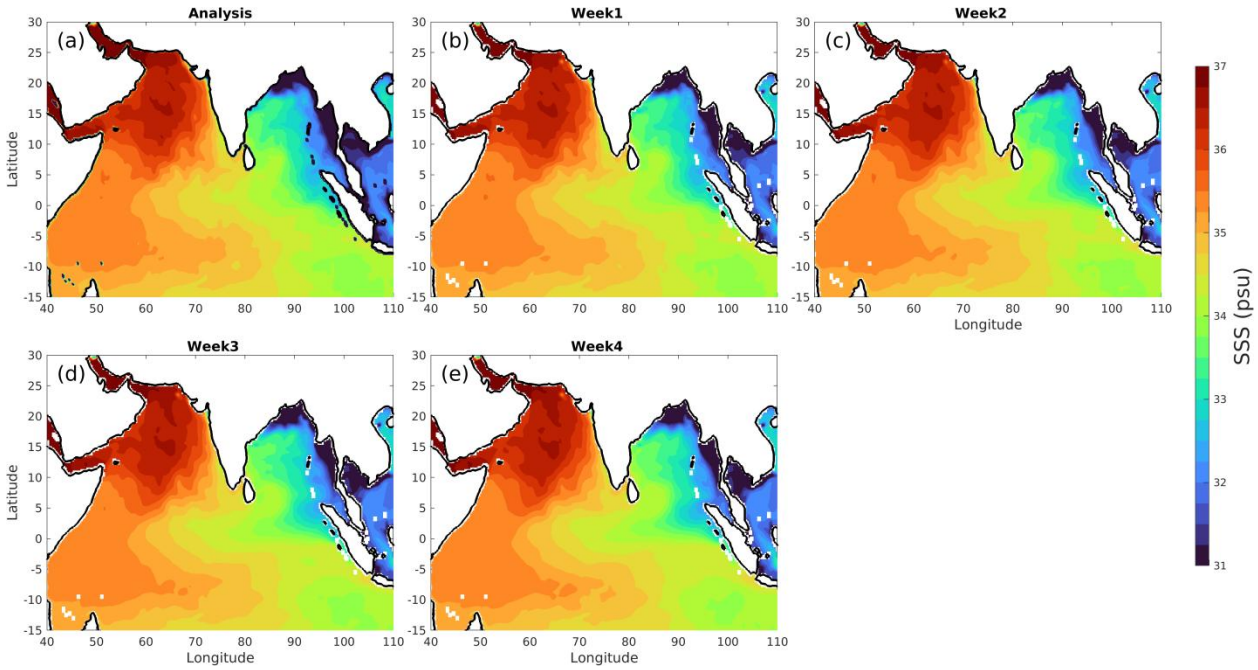

Figure 6 Mean SSS (psu) during JJAS. (a) Model-analysis for dates falling within week-1 of model initialization. b), c), d), and e) SST for week-1, 2, 3 and 4 forecasts, respectively

4.2 Sea Surface Salinity

As discussed above, fresh water fluxes and contrast in salinity structure of the two basins are some of the unique features of the north Indian Ocean. Due to its importance on the upper ocean thermohaline structure, we now discuss the salinity forecasts during the 2023 JJAS. The seasonal mean of the sea surface salinity (SSS) for monsoon season (JJAS) is shown in Figure 6a. We observe that the AS has higher SSS (~37 psu) than BOB. The northern BOB has particularly low SSS values (~28 psu) during monsoon season as a result of increased freshwater transport from major adjoining rivers (Ganga, Brahmaputra and Irrawaddy) (Sengupta et al., 2006). The southern BOB has higher SSS than the northern BOB in this season. However, an opposite pattern is seen in AS where the north is much more saltier than the south AS. It is well known that the fresh waters and low salinity in the BOB are due to the excess precipitation over evaporation as well as river discharge. Similarly, the excess evaporation over precipitation combined with vertical mixing of high salinity subsurface water masses maintains high surface salinity in much of the AS. The low salinity seen in the southern AS is mainly contributed by the advection of fresh water from the southern hemisphere along the Somali Jet. It can be seen from Figure 6 b-e that the model captures these spatial distributions of the salinity remarkably well even in week-4 forecasts.

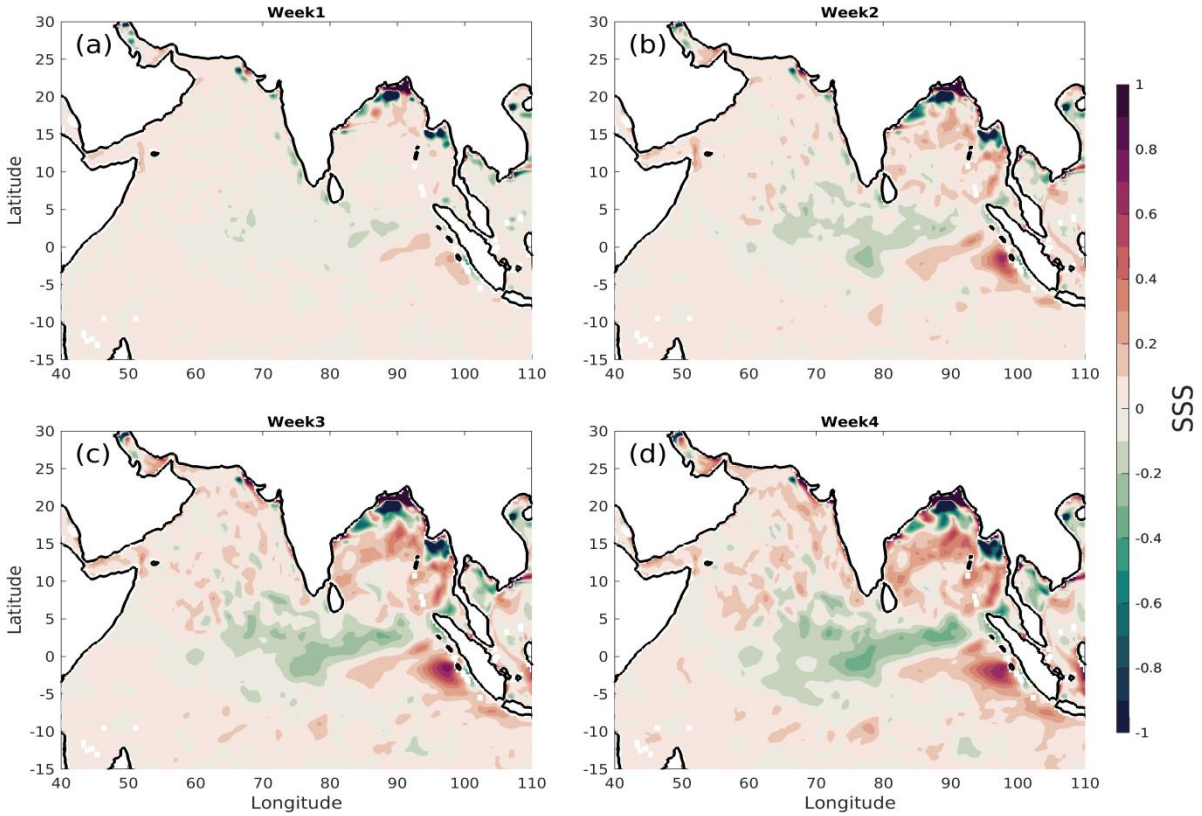

Figure 7 SSS biases (psu) for (a) week-1, (b) week-2, (c) week-3 and (d) week-4 forecast.

Figure 7 shows the biases in SSS in week-1 to week-4 forecasts. It can be seen that less than 0.1 psu of biases exist in week-1 except the head BOB. By week-4 substantial biases of the order of ~0.5 psu develops over large parts of the BOB and east AS. It may be noted that SSS biases are negative over the head BOB. Thus the positive SSS biases in the interior of the BOB could be due to reduced freshwater flux (evaporation and precipitation) in the model as well as reduced advection of fresh water from the north BOB. Since salinity is an important factor in determining the upper ocean stratification, existence of biases of opposite nature within a small region of BOB warrants further study. A similar dipole in SSS biases are seen over equatorial Indian Ocean where positive SSS biases over the SEEIO exists alongside the negative SSS biases to the west. It may be noted that SEEIO is usually a region of low salinity waters. Thus, the existence of dipole in SSS biases over SEEIO could suggest anomalous advection of freshwater towards the west and upwelling of saltier subsurface waters over the SEEIO. These results can also be

corroborated by pattern of SST biases which also suggest cooling due to anomalous upwelling over the SEEIO.

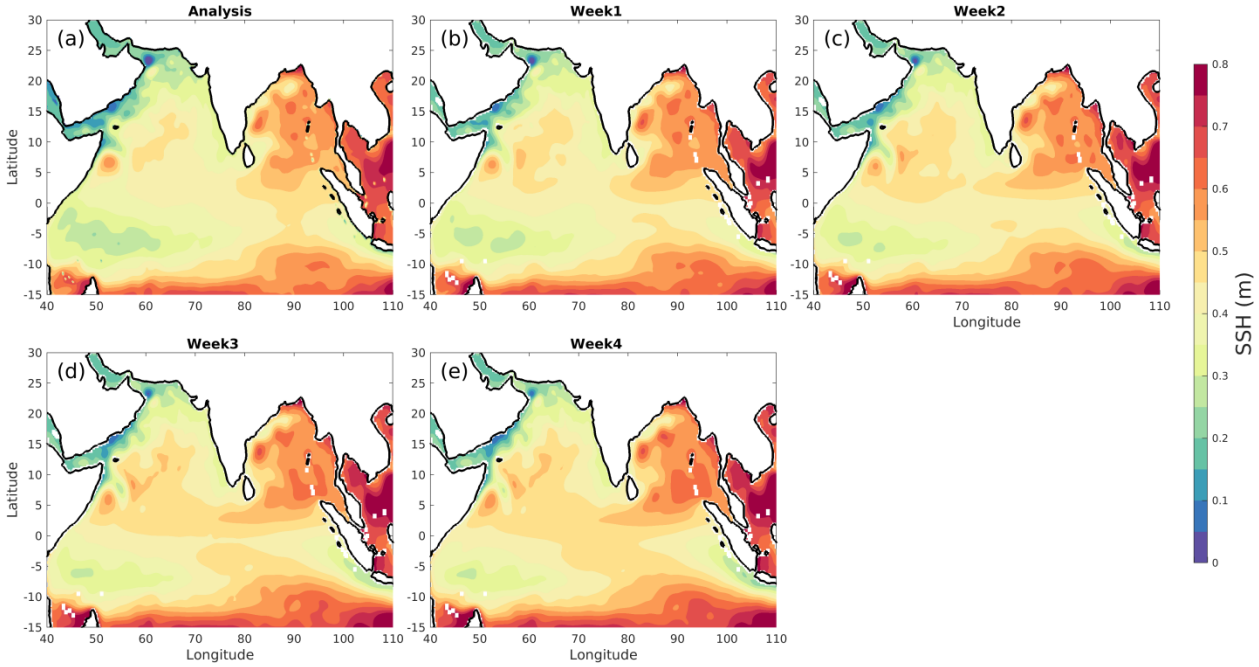

Figure 8 Mean SSH (m) during JJAS. (a) Model-analysis for dates falling within week-1 of model initialization. b), c), d), and e) SST for week-1, 2, 3 and 4 forecasts, respectively

4.3 Sea Surface Height

The large scale circulation of the Indian Ocean is dominated by local winds as well as locally and remotely generated waves. The signature of these surface waves can be clearly seen in the sea surface heights (SSH). Moreover, the changes in SSH reflects the cumulative effects of vertically integrated changes in salinity and temperature profiles in the water column which may result from global warming and associated water flux into the oceans. The upper ocean heat content is also tied closely with the SSH (Momin et al., 2021). Due to the potential effects of SSH on the upper ocean heat content and thus air-sea interactions in the region, it is important to analyze the performance of coupled models in capturing the patterns of SSH (Gera et al., 2016). The SSH during JJAS season is shown in Figure 8. A contrast in mean SSH between AS and the

BOB can be seen. It is known that during the pre-monsoon the equatorial Indian Ocean region is under the influence of westerly wind bursts which force downwelling Kelvin waves which propagates as coastally trapped downwelling Kelvin waves along the periphery of the BOB. The increased SSH along the east coast of BOB along with local winds can further force westward traveling Rossby waves into the interior of the bay. These processes are responsible for higher SSH in the BOB compared to AS (Gera et al., 2016). A low in SSH is particularly observed along the west coast of AS where it is related to Ekman suction induced by strong monsoonal winds. Further, the southwestern equatorial Indian Ocean shows another trough in SSH at latitudes from 5° S to 15°S. This feature is known in literature at dome of low SSH and sits over a climatological upwelling zone where mean sea level is lower than in the nearby areas (McCreary et al., 1993). The model consistently captures the observed pattern of SSH in week-1 to week-4 forecast as illustrated in Figure Figure 8 b-e). Moreover in week-2 to week-4, slightly higher SSH values over the central BOB are observed compared to week-1 forecast as well as observation.

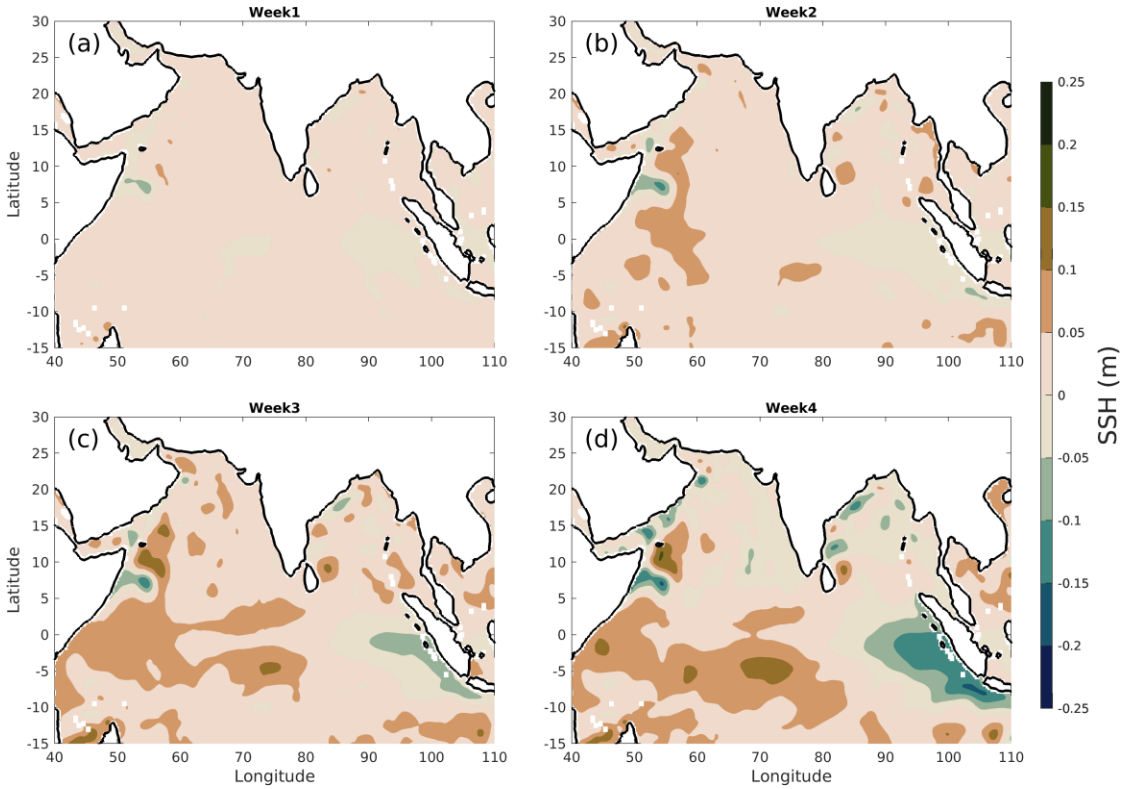

Figure 9 SSH biases (m) for (a) week-1, (b) week-2, (c) week-3 and (d) week-4 forecast

To analyze the errors in the model, SSH biases are plotted in Figure 9. It can be seen that the model shows only limited biases up to week-3. In week-4 forecast too except for region of Somali jet, most biases are limited to the equatorial region. As discussed above the circulation in the Indian Ocean is sensitive to the equatorial SSH, thus biases in SSH in the region could potentially affect the temperature, salinity and current biases elsewhere in the region. A close look at week-4 forecast highlights the dipole in SSH. While positive SSH biases are present in the west, negative SSH biases are present in the east – a pattern which is reminiscence of the positive Indian Ocean dipole. It may be noted that both the SST and SSS biases discussed above are thus consistent the internal dynamics of the equatorial Indian Ocean.

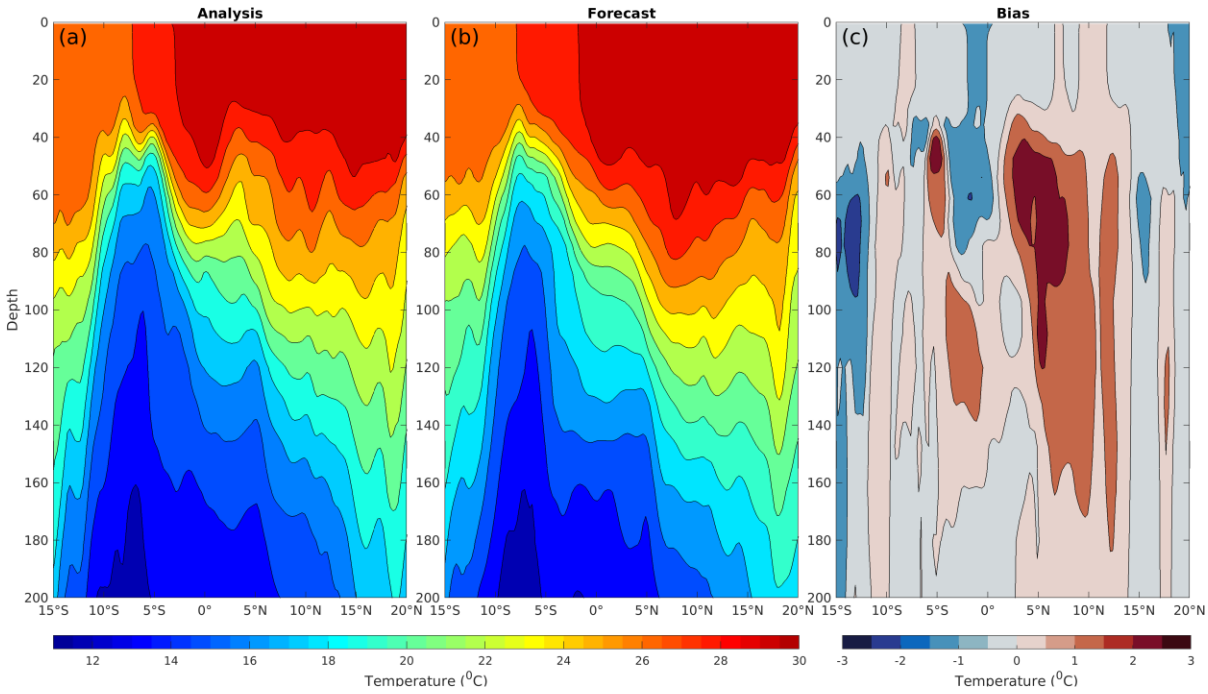

Figure 10 Temperature cross-section profile over Arabian Sea

5 Subsurface structure of the north Indian Ocean during June

In an effort to demonstrate the quality of sub-surface model fields, we compare the meridional cross-section (latitude-depth map) of monthly-mean model derived temperature at 65° E in the AS and 90° E in the BOB against the model-analysis for June 2023 in Figure 10 and Figure 11, respectively. It can be seen that temperatures in both AS and BOB are warmer in the north compared to the south. For the AS, temperatures above 20^{o}C are restricted to upper 50 m in the south but are present even at the depths of ~ 120 m in the north (Figure 10). Thus the thermocline shows a steep downward slope towards the north in the AS. Further south of 5-10^{o}S the thermocline deepens towards the south. Thus a steep shoaling of thermocline is seen at the latitudes 5-10^{o}S which as discussed above is an important area of open-ocean upwelling in the Indian Ocean and act a region which is sensitive to the air-sea coupling (Schott & McCreary, 2001; Yokoi et al., 2008). The deeper thermoclines of the north also means that the ocean act as much larger reservoir of heat in the north AS providing continuous supply of moisture all through the monsoon season via latent heat fluxes. It can be seen the model realistically captures the thermocline structure of the upper ocean (Figure 10b), although the warmest temperatures

exist much more deeper in the model compared to the analysis over AS. This results in warm temperature bias at the depths of 40-60 m in the AS (Figure 10c).

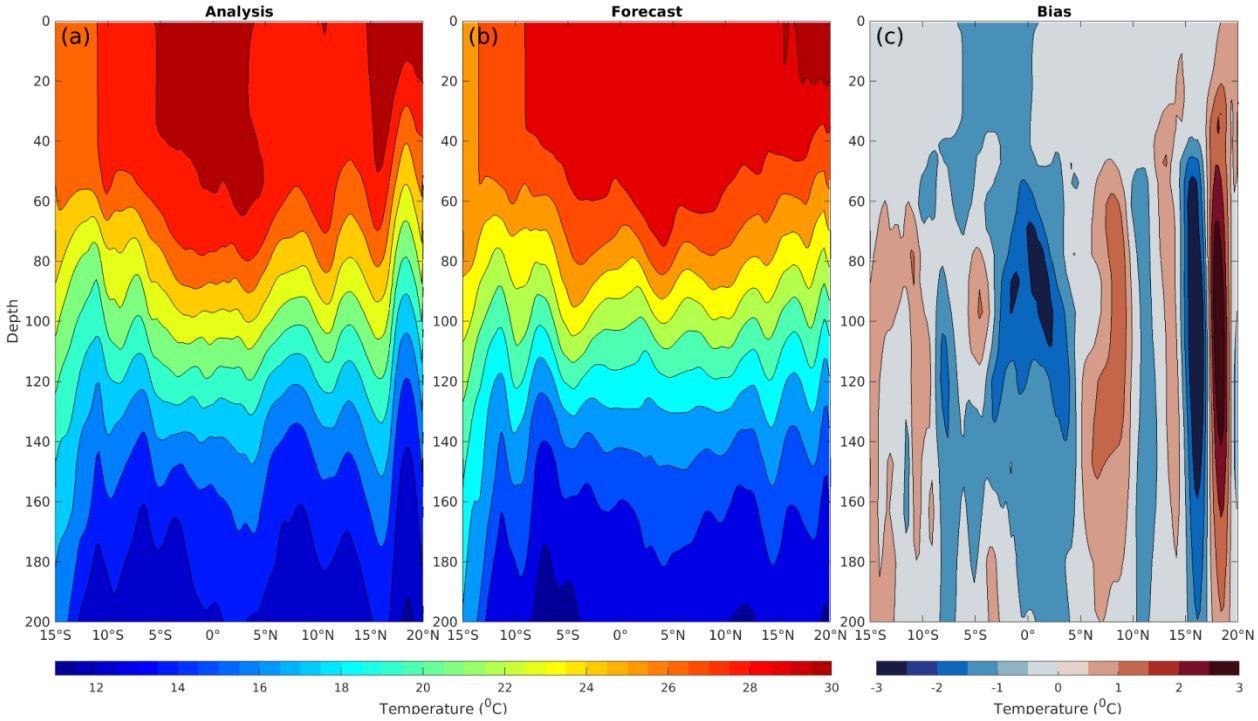

Figure 11 Temperature cross-section profile over Bay of Bengal

In contrast, much milder slopes of thermoclines are seen in the BOB (Figure 11); in fact, the thermoclines are nearly flat for much of the BOB. However, a steep shoaling of thermocline can also be seen in the BOB towards the north-most latitudes. While the associated upwelling is less studied, it may be related to the existence of semi-permanent cyclonic eddy which is present north of 15^{o}N during most of the summer season (not shown). Further, a bimodal structure of temperatures is seen in the BOB with peak near-surface temperatures present both over the equatorial region as well as the head BOB. As seen in Figure 1, this is mainly due to the presence of extremely warm temperatures in the head BOB and SEEIO before the monsoonal winds gains their peak during July-August and brings down the temperature all over the bay. It may be interesting to note that while MLD are very shallow in the BOB the depth of thermocline is quite deep. The model forecasts temperature stratification quite realistically in the upper ocean in BOB with correct magnitude of temperatures (Figure 11b). A pattern of warm and cold sub-surface biases are present in depths from 50-150 m just below the thermocline and may suggest the influence of waves propagating from the equatorial region.

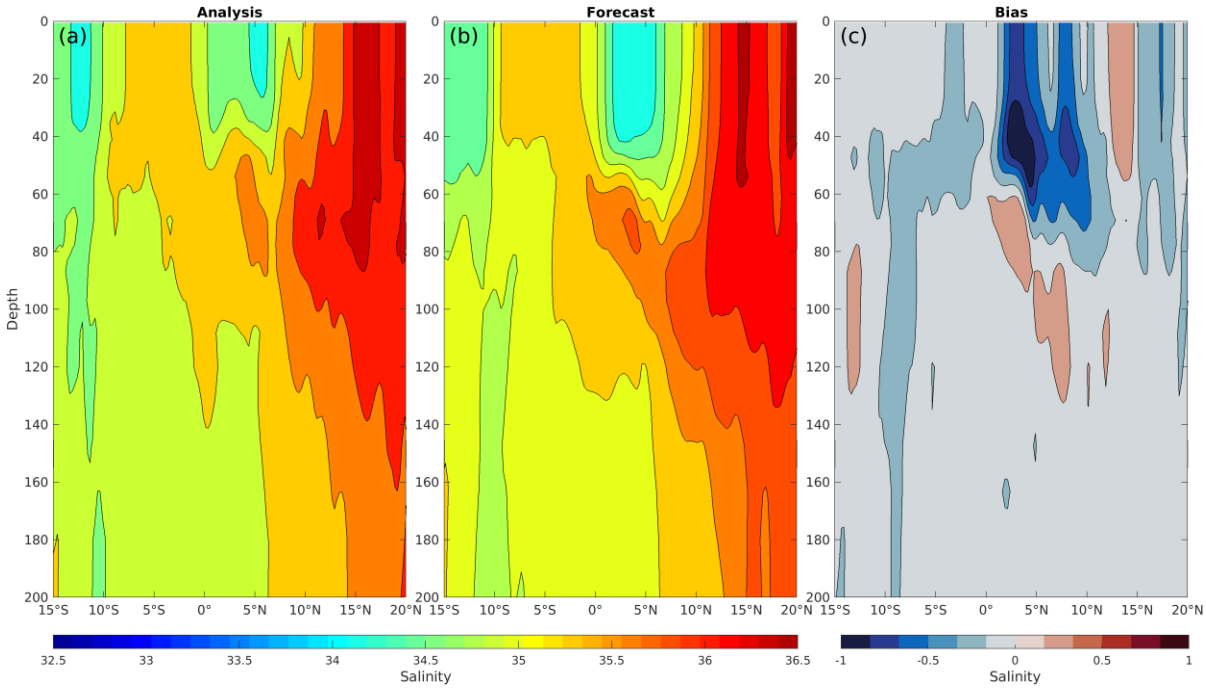

Figure 12 Salinity cross-section profile over Arabian Sea

To demonstrate the quality of model simulation in representing the sub-surface characteristics of salinity, we show in latitude-depth maps of salinity at 65°E in the AS and 90°E in the BOB in Figure 12 and Figure 13, respectively. The sub-surface salinity structures are very different in the AS and BOB. The salinity diagram shows that the north-south gradient of salinity is nearly opposite in the AS and BOB. For example, in the region 10°–20°N, where the highest salinity values are observed in the AS, the BOB region shows the lowest salinity. The low salinity of the BOB in this region is mainly attributed to freshening of water as a result of river runoff from major adjoining rivers of the region. On the other hand, higher evaporation over precipitation in the northern AS is the principal reason of high salinity in that region. The presence of salty outflow from the Red Sea and Persian Gulf is also the reason for high salinity in north AS. From 5-15^{o}N a sub-surface salinity maximum is also observed. The model forecast for the month of June correctly captures the north-south gradient of salinity in both AS and BOB (Figure 12b and Figure 13b). However, it can be observed that the model forecast is underestimated approx ~1 psu over 5^{0}N-10^{0}N up to 50m depth for AS (Figure 12c) and overestimated by ~1 psu over the head BOB up to 50m depth (Figure 13c).

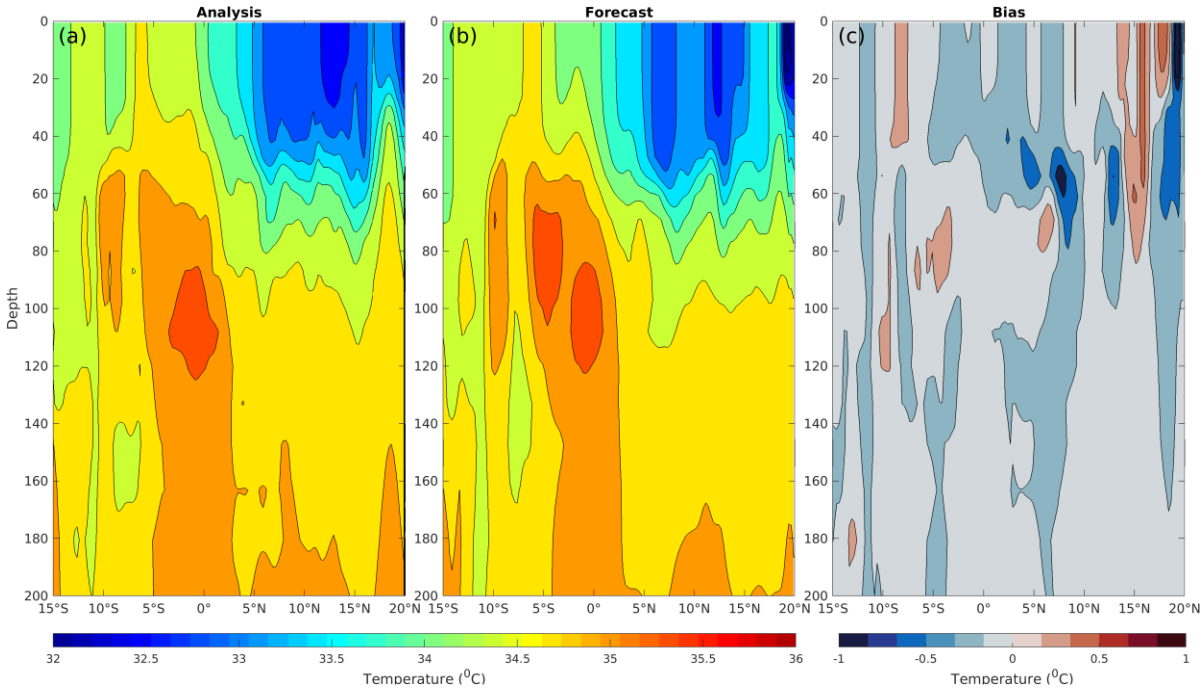

Figure 13 Salinity cross-section profile over Bay of Bengal

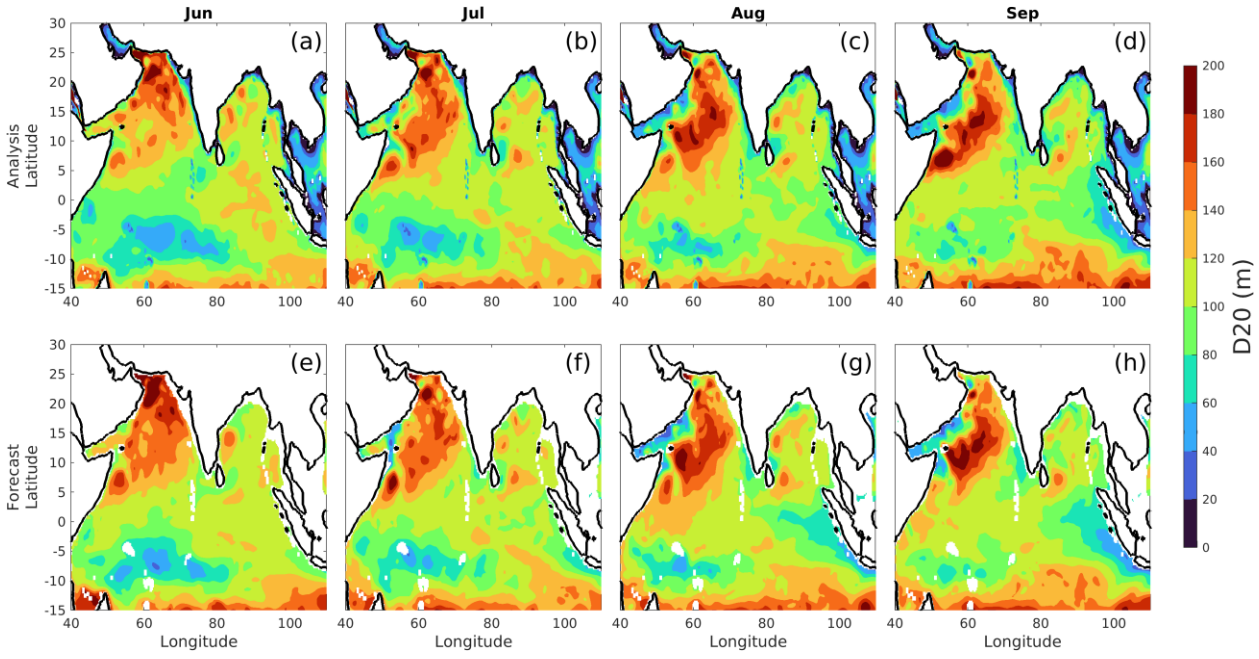

Figure 14 Depth of 20°C isotherm (D20) during a) and e) June, b) and f) July, c) and g) August, and d) and h) September as estimated from a-d) model analysis. D20 forecasted by the coupled model initialized in the last week of the month preceding the validity month are shown in e-h).

6 Monthly-mean thermodynamic features

In addition to the substantial sea surface temperature variability, subsurface temperature also have significant variability caused by the changes in the thermocline of the ocean (Rao et al., 2009; Yu, 2003) and varying induced mixing impacted by variable atmospheric forcing (Keerthi et al., 2013; Srivastava et al., 2018) . The thermocline is greatly influenced by westward propagating equatorial Rossby waves, eastward propagating equatorial Kelvin waves over equatorial region and poleward propagating coastal Kelvin wave along the eastern boundary of BOB (Kessler, 1991; White, 1977 and references therein). The skill of the model in simulating these waves can be demonstrated using 20 degree isotherm (D20) (Murtugudde et al., 2000) . We have investigated the D20 for model as well as analysis during June 2023 (Figure 11). Figure 14 reveals large spatial variability of D20 over study domain. The magnitude of the deepening of D20 varies spatially and deepening and shoaling over different regions is influenced by different dynamical processes. We noticed shoaling of thermocline off the coasts of Somalia and Arabia caused by the strong upwelling over the same region during June 2023. This is supported by the previous studies of Schott, 1983, Schott & McCreary, 2001, and Weller et al., 2002. The shoaling of the D20 over the equatorial region signifies the presence of weak equatorial Kelvin waves. The shoaling of the D20 over southern tropical Indian Ocean south of 5^{o}S is associated with strengthening of the Ekman divergence caused by enhanced cyclonic gyre (CG)(Murtugudde & Busalacchi, 1999; Yokoi et al., 2009) . In this region, the negative wind curl between the southeasterly trades and equatorial westerlies raises the thermocline, leading to open-ocean upwelling (Xie et al., 2002). It can be also observed that the high value of D20 over the AS as compared to the BOB.

Model forecast for JJAS 2023 shows realistic skill in reproducing this spatial variability of the D20 and their changing nature (Figure 14e-f). However, the model forecasts slightly deeper D20 in the AS during June and deeper D20 over the WEIO and shallower D20 over SEEIO during August and September. Over the equatorial Indian Ocean deeper D20 biases in the west and shallower D20 biases in the east are consistent with positive SSH biases in west and negative SSH biases in the east and are indicative of involvement of equatorial Rossby waves (Figure 9).

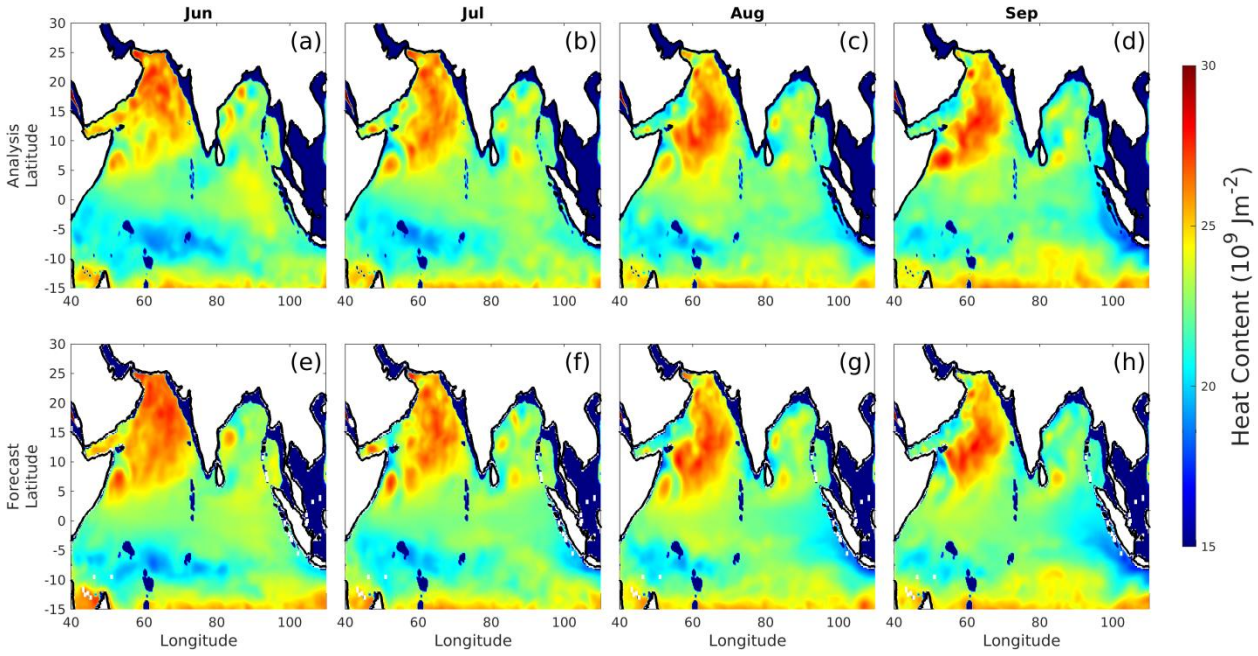

Figure 15 Heat content in upper 300m of the ocean (HC300) during a) and e) June, b) and f) July, c) and g) August, and d) and h) September as estimated from a-d) model analysis. HC300s forecasted by the coupled model initialized in the last week of the month preceding the validity month are shown in e-h).

The depth of themocline is an important variable indicative of the heat storage in the upper ocean. It can be seen from Figure 15 that the spatial pattern of the vertically integrated heat content in the upper 300m (HC300) of the ocean is similar to the D20 spatial pattern. Higher heat content is seen in the AS as compared to the BOB. The effect of shallower D20 over from 5-15^{o}S is also seen as low HC300 over the region. Local peaks in HC300 is also observed over different regions of the AS and BOB are seen to be collocated with deeper D20 and are associated with anticyclonic eddies in the region.

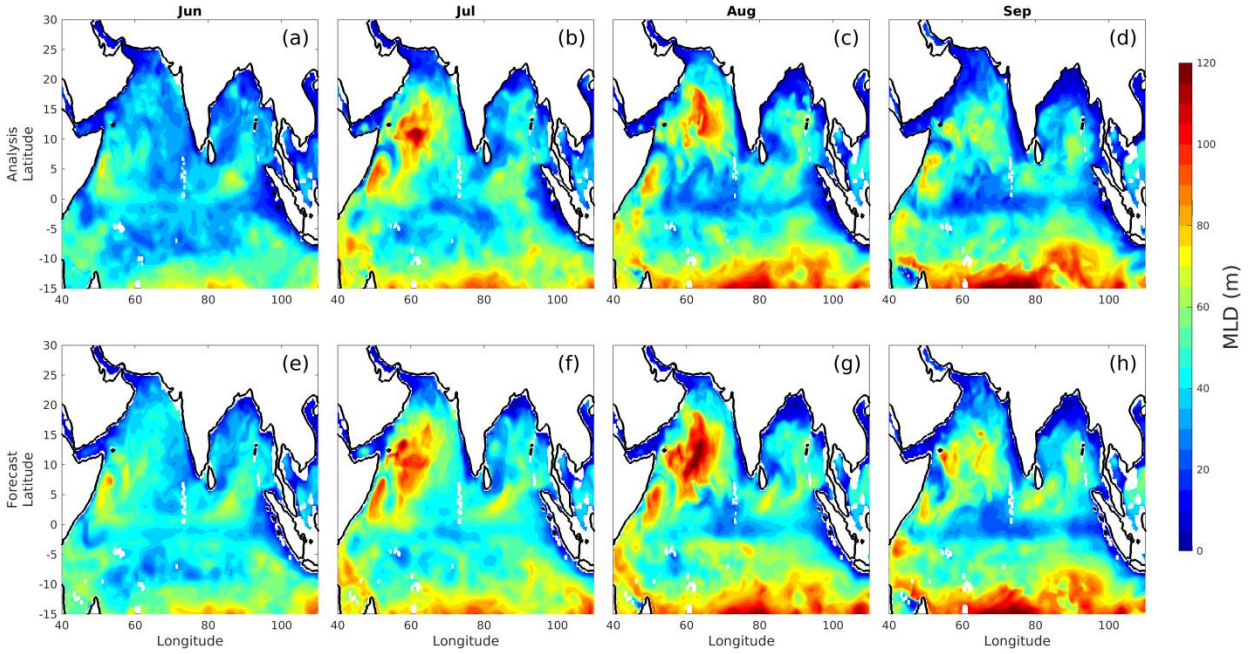

Figure 16 Mixed layer depths (MLD) during a) and e) June, b) and f) July, c) and g) August, and d) and h) September as estimated from a-d) model analysis. MLD forecasted by the coupled model initialized in the last week of the month preceding the validity month are shown in e-h).

Finally, Figure 16 shows the mixed layer depths (MLD) estimated from the model analysis and model forecasts for each of the month of JJAS. MLD is an important diagnostic of the upper ocean mixing. The variations in MLD are due to the combined impacts of surface momentum and buoyancy fluxes as well as the stratification of the ocean. Unlike D20 and HC300, large variations in the monthly-mean MLD are seen. Highest MLD are seen over the AS in the month of July and August with June showing the least of MLD. Compared to BOB much deeper MLD are seen in AS in any given month. The deeper MLD in the AS are result of strong turbulent mixing by monsoonal winds in the presence of much weaker stratification as compared to BOB (Figure 10). In comparison, the monsoonal winds are weaker over the BOB and the upper ocean is much more stratified compared to AS particularly when one looks into the salt stratification (Figure 11and Figure 13). These differences result in monsoonal winds being able to mix much deeper waters of the AS in comparison with the BOB. Model simulates the monthly variations in the MLD in both AS and BOB, although, the MLD in the model are slightly higher in the AS.

7 Discussion on model performance in simulating ocean features

In this study the performance of the extended range forecast system at NCMRWF in simulating the upper ocean features in 2023 summer monsoon season is analyzed. Focus is made on the large scale patterns of SST, SSS, SSH, and upper ocean heat content. By comparing the forecasts with observations and model analysis systematic biases in the key ocean variables are also studied. It is found that the model captures the spatial pattern of upper ocean thermodynamic variables reasonably well in week-1 to week-4 forecasts. It is found that the model captures the seasonal cycle of SST but shows large cooling tendency particularly over SEEIO. It is interesting to note that substantial biases are present in week-1 itself. Such early appearance of biases could partly be contributed by errors in model-analysis, atmospheric forcings, and representation of upper ocean thermo-dynamical processes. However, biases in some regions in the Indian Ocean increases sharply by week-4 indicative of model errors. The biases in SST, SSS, and SSH show an east-west dipole structure over the equatorial regions. The subsurface structure and upper ocean stratification of temperature and salinity has also been captured well in forecasts. However, large biases in temperature and salinity are seen near the thermocline region suggesting the importance of mixing processes in determining the near-surface ocean variables. Based on the analysis of 2023 summer season it is found that while model captures the processes determining the large scale spatial pattern, however, the consideration of existences of systematic biases must be done while making informed decision regarding ocean forecast. The results of this analysis help in identifying the areas for model improvement and provide feedback for future development of the coupled model.

Authors Contributions

LP generated the plots and analyzed the results, AG conceptualized the study and wrote the manuscript, and AKM guided the study. All authors participated in interpretation of results and editing and revising the manuscript.

References

Abhilash, S., Sahai, A. K., Borah, N., Chattopadhyay, R., Joseph, S., Sharmila, S., De, S., Goswami, B. N., & Kumar, A. (2014). Prediction and monitoring of monsoon intraseasonal

oscillations over Indian monsoon region in an ensemble prediction system using CFSv2. *Climate Dynamics*. https://doi.org/10.1007/s00382-013-2045-9

Amante, C., & Eakins, B. W. W. (2009). ETOPO1 – 1 arc-minute global relief model: Procedures, data sources and analysis. In *NOAA Technical Memorandum NESDIS NGDC-24*. https://doi.org/10.1594/PANGAEA.769615

Anand, A., Mishra, S. K., Sahany, S., Bhowmick, M., Rawat, J. S., & Dash, S. K. (2018). Indian Summer Monsoon Simulations: Usefulness of Increasing Horizontal Resolution, Manual Tuning, and Semi-Automatic Tuning in Reducing Present-Day Model Biases. *Scientific Reports*, *8*(1). https://doi.org/10.1038/s41598-018-21865-1

Belcher, S. E., Hewitt, H. T., Beljaars, A., Brun, E., Fox-Kemper, B., Lemieux, J.-F., Smith, G., & Valcke, S. (2015). Ocean--waves--sea ice--atmosphere interactions. *Seamless Prediction of the Earth System: From Minutes to Months, Eds G. Brunet, S. Jones, and PM Ruti (Geneva: World Meteorological Organization, 2015).*

Davis, R. E., Talley, L. D., Roemmich, D., Owens, W. B., Rudnick, D. L., Toole, J., Weller, R., McPhaden, M. J., & Barth, J. A. (2018). 100 years of progress in ocean observing systems. *Meteorological Monographs, 59*. https://doi.org/10.1175/AMSMONOGRAPHS-D-18-0014.1

De Boyer Montégut, C., Vialard, J., Shenoi, S. S. C., Shankar, D., Durand, F., Ethé, C., & Madec, G. (2007). Simulated seasonal and interannual variability of the mixed layer heat budger in the Northern Indian ocean. *Journal of Climate*, *20*(13). https://doi.org/10.1175/JCLI4148.1

Du, Y., Qu, T., & Meyers, G. (2008). Interannual variability of sea surface temperature off Java and Sumatra in a global GCM. *Journal of Climate*, *21*(11). https://doi.org/10.1175/2007JCLI1753.1

Dwivedi, S., Goswami, B. N., & Kucharski, F. (2015). Unraveling the missing link of ENSO control over the Indian monsoon rainfall. *Geophysical Research Letters*, *42*(19). https://doi.org/10.1002/2015GL065909

Dwivedi, S., Mittal, A. K., & Goswami, B. N. (2006). An empirical rule for extended range prediction of duration of Indian summer monsoon breaks. *Geophysical Research Letters*, *33*(18). https://doi.org/10.1029/2006GL027035

Findlater, J. (1969). A major low-level air current near the Indian Ocean during the northern summer. *Quarterly Journal of the Royal Meteorological Society*, *95*(404). https://doi.org/10.1002/qj.49709540409

Gadgil, S, & Gadgil, S. (2006). The Indian monsoon, GDP and agriculture. *Econ. Polit. Weekly*, 4887–4895.

Gadgil, Sulochana. (2003). The Indian monsoon and its variability. *Annual Review of Earth and Planetary Sciences*, *31*. https://doi.org/10.1146/annurev.earth.31.100901.141251

Gadgil, Sulochana, Joseph, P. V, & Joshi, N. V. (1984). Ocean--atmosphere coupling over monsoon regions. *Nature*, *312*(5990), 141–143.

Gadgil, Sulochana, Rajeevan, M., & Nanjundiah, R. (2005). Monsoon prediction—why yet another failure. *Curr. Sci*, *88*(9), 1389–1400.

George, J. P., Rani, S. I., Jayakumar, A., Mohandas, S., Mallick, S., Lodh, A., Rakhi, R., Sreevathsa, M. N. R., & Rajagopal, E. N. (2016). *NCUM data assimilation system*.

Gera, A., Gupta, A., Mitra, A. K., Rao D., N., Momin, I. M., Rajeeavan, M. N., Milton, S. F., Martin, G. M., Martin, M. J., Waters, J., & Lea, D. (2022). Skill of the extended range prediction (NERP) for Indian summer monsoon rainfall with NCMRWF global coupled modelling system. *Quarterly Journal of the Royal Meteorological Society*, *148*(742). https://doi.org/10.1002/qj.4216

Gera, A., Mitra, A. K., Mahapatra, D. K., Momin, I. M., Rajagopal, E. N., & Basu, S. (2016). Sea surface height anomaly and upper ocean temperature over the Indian Ocean during contrasting monsoons. *Dynamics of Atmospheres and Oceans*, *75*. https://doi.org/10.1016/j.dynatmoce.2016.04.002

Goswami, B. N., Rao, S. A., Sengupta, D., & Chakravorty, S. (2016). Monsoons to mixing in the

Bay of Bengal: Multiscale air-sea interactions and monsoon predictability. *Oceanography*, *29*(2). https://doi.org/10.5670/oceanog.2016.35

Gupta, A., Mitra, A. K., & Rajagopal, E. N. (2019). Implementation of Sub-Seasonal to Seasonal Forecast System with NCMRWF Global Coupled Model. *NCMRWF Technical Report*, *NMRF/TR/04*, 70.

Gupta, A., Pandey, A. C., & Mitra, A. K. (2022). Development of early sea surface temperature biases in the tropical Indian Ocean in a coupled model. *Dynamics of Atmospheres and Oceans*, *97*, 101269.

Hunke, E. C., & Dukowicz, J. K. (1997). An elastic--viscous--plastic model for sea ice dynamics. *Journal of Physical Oceanography*, *27*(9), 1849–1867.

Imranali, M., Ashis, M., & E.N, R. (2020). Implementation of NEMO based Global 3D- Var Ocean Data Assimilation System at NCMRWF: Technical Aspects. In *Implementation of NEMO based Global 3D- Var Ocean Data Assimilation System at NCMRWF: Technical Aspects* (Issue June).

IOC, I. H. O., & In, B. (2003). Centenary edition of the GEBCO digital atlas, published on CD-ROM on behalf of the Intergovernmental Oceanographic Commission and the International Hydrographic Organization as part of the General Bathymetric Chart of the Oceans. *British Oceanographic Data Centre*.

Izumo, T., Montegut, C. de B., Luo, J. J., Behera, S. K., Masson, S., & Yamagata, T. (2008). The role of the Western Arabian Sea upwelling in Indian monsoon rainfall variability. *Journal of Climate*, *21*(21). https://doi.org/10.1175/2008JCLI2158.1

Kara, A. B., Rochford, P. A., & Hurlburt, H. E. (2000). An optimal definition for ocean mixed layer depth. *Journal of Geophysical Research: Oceans*, *105*(C7). https://doi.org/10.1029/2000jc900072

Keerthi, M. G., Lengaigne, M., Vialard, J., & de Boyer Montégut, C Muraleedharan, P. M. (2013). Interannual variability of the Tropical Indian Ocean mixed layer depth. *Climate Dynamics*, *40*(3), 743–759.

Kelly, K. A., Small, R. J., Samelson, R. M., Qiu, B., Joyce, T. M., Kwon, Y.-O., & Cronin, M. F. (2010). Western boundary currents and frontal air--sea interaction: Gulf Stream and Kuroshio Extension. *Journal of Climate*, *23*(21), 5644–5667.

Kessler, W. S. (1991). Can Reflected Extra-equatorial Rossby Waves Drive ENSO? *Journal of Physical Oceanography*, *21*(3). https://doi.org/10.1175/1520-0485(1991)021<0444:creerw>2.0.co;2

Klingaman, N. P., & Woolnough, S. J. (2014). The role of air--sea coupling in the simulation of the Madden--Julian oscillation in the Hadley Centre model. *Quarterly Journal of the Royal Meteorological Society*, *140*(684), 2272–2286.

Koul, V., Parekh, A., Srinivas, G., Kakatkar, R., Chowdary, J. S., & Gnanaseelan, C. (2018). Role of Ocean Initial Conditions to Diminish Dry Bias in the Seasonal Prediction of Indian Summer Monsoon Rainfall: A Case Study Using Climate Forecast System. *Journal of Advances in Modeling Earth Systems, 10*(3). https://doi.org/10.1002/2017MS001129

Kumar, S., Bushair, M. T., Buddhi Prakash, J., Lodh, A., Sharma, P., George, G., Rani, S. I., George, J. P., Jayakumar, A., Mohandas, S., & others. (2020). NCUM Global NWP System: Version 6 (NCUM-G: V6). *NCMRWF Technical Report, NMRF/TR/06/2020*.

Ma, X., Chang, P., Saravanan, R., Montuoro, R., Nakamura, H., Wu, D., Lin, X., & Wu, L. (2017). Importance of resolving Kuroshio front and eddy influence in simulating the North Pacific storm track. *Journal of Climate*, *30*(5), 1861–1880.

Madec, G. (2008). NEMO – the OPA9 ocean engine: Note du Pole de Modelisation. *Institut Pierre-Simion Laplace, 1:100, Available at: Http://Www.Nemo-Ocean.Eu, Last Access: 18 November 2013, 2008.*

McCreary, J. P., Kundu, P. K., & Molinari, R. L. (1993). A numerical investigation of dynamics, thermodynamics and mixed-layer processes in the Indian Ocean. *Progress in Oceanography*, *31*(3), 181–244. https://doi.org/10.1016/0079-6611(93)90002-U

Megann, A., Storkey, D., Aksenov, Y., Alderson, S., Calvert, D., Graham, T., Hyder, P., Siddorn, J., & Sinha, B. (2014). GO5.0: The joint NERC-Met Office NEMO global ocean

model for use in coupled and forced applications. *Geoscientific Model Development*, *7*(3), 1069–1092. https://doi.org/10.5194/gmd-7-1069-2014

Mesinger, F., & Arakawa, A. (1976). *Numerical methods used in atmospheric models*.

Mishra, A. K., Dwivedi, S., & Das, S. (2020). Role of Arabian Sea warming on the Indian summer monsoon rainfall in a regional climate model. *International Journal of Climatology*, *40*(4). https://doi.org/10.1002/joc.6328

Momin, I. M., Karmakar, A., Gupta, A., & Mitra, A. K. (2021). Tropical cyclone heat potential (Tchp) from the ncmrwf nemo based global ocean analysis and forecast system. *Mausam*, *72*(1). https://doi.org/10.54302/mausam.v72i1.136

Murtugudde, R., & Busalacchi, A. J. (1999). Interannual variability of the dynamics and thermodynamics of the tropical Indian Ocean. *Journal of Climate*, *12*(8 PART 1). https://doi.org/10.1175/1520-0442(1999)012<2300:ivotda>2.0.co;2

Murtugudde, Raghu, McCreary, J. P., & Busalacchi, A. J. (2000). Oceanic processes associated with anomalous events in the Indian Ocean with relevance to 1997-1998. In *Journal of Geophysical Research: Oceans* (Vol. 105, Issue C2). https://doi.org/10.1029/1999jc900294

Prasad, T. G. (2004). A comparison of mixed-layer dynamics between the Arabian Sea and Bay of Bengal: One-dimensional model results. *Journal of Geophysical Research: Oceans*, *109*(3). https://doi.org/10.1029/2003jc002000

Rae, J. G. L., Hewitt, H. T., Keen, A. B., Ridley, J. K., West, A. E., Harris, C. M., Hunke, E. C., & Walters, D. N. (2015). Development of the Global Sea Ice 6.0 CICE configuration for the Met Office Global Coupled model. *Geoscientific Model Development*, *8*(7), 2221–2230. https://doi.org/10.5194/gmd-8-2221-2015

Rajeevan, M., Pai, D. S., Kumar, R. A., & Lal, B. (2007). New statistical models for long-range forecasting of southwest monsoon rainfall over India. *Climate Dynamics*, *28*(7–8), 813–828.

Rajeevan, M., Unnikrishnan, C. K., & Preethi, B. (2012). Evaluation of the ENSEMBLES multi-model seasonal forecasts of Indian summer monsoon variability. *Climate Dynamics*, *38*(11–

12), 2257–2274.

Rao, R. R., & Sivakumar, R. (1999). On the possible mechanisms of the evolution of a mini-warm pool during the pre-summer monsoon season and the genesis of onset vortex in the South-Eastern Arabian Sea. *Quarterly Journal of the Royal Meteorological Society*, *125*(555). https://doi.org/10.1002/qj.49712555503

Rao, S. A., Dhakate, A. R., Saha, S. K., Mahapatra, S., Chaudhari, H. S., Pokhrel, S., & Sahu, S. K. (2012). Why is Indian Ocean warming consistently? *Climatic Change*, *110*(3–4). https://doi.org/10.1007/s10584-011-0121-x

Rao, S. A., Luo, J. J., Behera, S. K., & Yamagata, T. (2009). Generation and termination of Indian Ocean Dipole events in 2003, 2006 and 2007. *Climate Dynamics*, *33*(6). https://doi.org/10.1007/s00382-008-0498-z

Rao, S. A., Pillai, P. A., Pradhan, M., & Srivastava, A. (2019). Seasonal prediction of indian summer monsoon in India: The past, the present and the future. *Mausam*, *70*(2). https://doi.org/10.54302/mausam.v70i2.171

Reynolds, R. W., Smith, T. M., Liu, C., Chelton, D. B., Casey, K. S., & Schlax, M. G. (2007). Daily high-resolution-blended analyses for sea surface temperature. *Journal of Climate*, *20*(22), 5473–5496.

Roxy, M. K., Ritika, K., Terray, P., & Masson, S. (2014). The curious case of Indian Ocean warming. *Journal of Climate*, *27*(22). https://doi.org/10.1175/JCLI-D-14-00471.1

Saha, S. K., Pokhrel, S., Chaudhari, H. S., Dhakate, A., Shewale, S., Sabeerali, C. T., Salunke, K., Hazra, A., Mahapatra, S., & Rao, A. S. (2014). Improved simulation of Indian summer monsoon in latest NCEP climate forecast system free run. *International Journal of Climatology*, *34*(5), 1628–1641.

Sahai, A. K., Mandke, S. K., Shinde, M. A., Chattopadhyay, R., Joseph, S., & Goswami, B. N. (200 C.E.). Experimental seasonal forecast of Indian summer monsoon 2007: statistical and dynamical models. *IITM Research Reports, RR120*.

Saji, N. H., Goswami, B. N., Vinayachandran, P. N., & Yamagata, T. (1999). A dipole mode in the tropical Indian ocean. *Nature*, *401*(6751). https://doi.org/10.1038/43854

Schott, F. (1983). Monsoon response of the Somali Current and associated upwelling. In *Progress in Oceanography* (Vol. 12, Issue 3). https://doi.org/10.1016/0079-6611(83)90014-9

Schott, F. A., & McCreary Jr, J. P. (2001). The monsoon circulation of the Indian Ocean. *Progress in Oceanography*, *51*(1), 1–123.

Schott, F. A., Xie, S.-P., & McCreary Jr, J. P. (2009). Indian Ocean circulation and climate variability. *Reviews of Geophysics*, *47*(1).

Sengupta, D., Bharath Raj, G. N., & Shenoi, S. S. C. (2006). Surface freshwater from Bay of Bengal runoff and Indonesian Throughflow in the tropical Indian Ocean. *Geophysical Research Letters*, *33*(22). https://doi.org/10.1029/2006GL027573

Shenoi, S. S. C., Shankar, D., & Shetye, S. R. (1999). On the sea surface temperature high in the Lakshadweep Sea before the onset of the southwest monsoon. *Journal of Geophysical Research: Oceans*, *104*(C7). https://doi.org/10.1029/1998jc900080

Shenoi, S. S. C., Shankar, D., & Shetye, S. R. (2002). Differences in heat budgets of the near-surface Arabian Sea and Bay of Bengal: Implications for the summer monsoon. *Journal of Geophysical Research: Oceans*, *107*(C6). https://doi.org/10.1029/2000jc000679

Srivastava, A., Dwivedi, S., & Mishra, A. K. (2018). Investigating the role of air-sea forcing on the variability of hydrography, circulation, and mixed layer depth in the Arabian Sea and Bay of Bengal. *Oceanologia*, *60*(2). https://doi.org/10.1016/j.oceano.2017.10.001

Subramanian, A., Balmaseda, M. A., Chattopadhyay, R., Centurioni, L. R., Cornuelle, B. D., DeMott, C., Hamill, T., Hendon, H., Hoteit, I., Flatau, M., Fujii, Y., Gille, S. T., Kumar, A., Lee, J. H., Lucas, D., Matsueda, M., Mahadevan, A., Nam, S. H., Paturi, S., … Zhang, C. (2019). Ocean observations to improve our understanding, modeling, and forecasting of subseasonal-to-seasonal variability. In *Frontiers in Marine Science* (Vol. 6, Issue JUL). https://doi.org/10.3389/fmars.2019.00427

Valcke, S. (2013). The OASIS3 coupler: A European climate modelling community software. *Geoscientific Model Development*, *6*(2), 373–388.

Vinayachandran, P. N., & Shetye, S. R. (1991). The warm pool in the Indian Ocean. *Proceedings of the Indian Academy of Sciences - Earth and Planetary Sciences*, *100*(2). https://doi.org/10.1007/BF02839431

Walters, D., Boutle, I., Brooks, M., Melvin, T., Stratton, R., Vosper, S., Wells, H., Williams, K., Wood, N., Allen, T., Bushell, A., Copsey, D., Earnshaw, P., Edwards, J., Gross, M., Hardiman, S., Harris, C., Heming, J., Klingaman, N., … Xavier, P. (2017). The Met Office Unified Model Global Atmosphere 6.0/6.1 and JULES Global Land 6.0/6.1 configurations. *Geoscientific Model Development*, *10*(4), 1487–1520. https://doi.org/10.5194/gmd-10-1487-2017

Wang, B., Xiang, B., Li, J., Webster, P. J., Rajeevan, M. N., Liu, J., & Ha, K. J. (2015). Rethinking Indian monsoon rainfall prediction in the context of recent global warming. *Nature Communications*, *6*. https://doi.org/10.1038/ncomms8154

Waters, J., Lea, D. J., Martin, M. J., Mirouze, I., Weaver, A., & While, J. (2015). Implementing a variational data assimilation system in an operational 1/4 degree global ocean model. *Quarterly Journal of the Royal Meteorological Society*, *141*(687), 333–349.

Webster, P. J., Magaña, V. O., Palmer, T. N., Shukla, J., Tomas, R. A., Yanai, M., & Yasunari, T. (1998). Monsoons: processes, predictability, and the prospects for prediction. *Journal of Geophysical Research: Oceans*, *103*(C7). https://doi.org/10.1029/97jc02719

Weller, R. A., Fischer, A. S., Rudnick, D. L., Eriksen, C. C., Dickey, T. D., Marra, J., Fox, C., & Leben, R. (2002). Moored observations of upper-ocean response to the monsoons in the Arabian Sea during 1994-1995. *Deep-Sea Research Part II: Topical Studies in Oceanography*, *49*(12). https://doi.org/10.1016/S0967-0645(02)00035-8

White, W. B. (1977). Annual Forcing of Baroclinic Long Waves in the Tropical North Pacific Ocean. *Journal of Physical Oceanography*, *7*(1). https://doi.org/10.1175/1520-0485(1977)007<0050:afoblw>2.0.co;2

Williams, K. D., Harris, C. M., Bodas-Salcedo, A., Camp, J., Comer, R. E., Copsey, D., Fereday, D., Graham, T., Hill, R., Hinton, T., Hyder, P., Ineson, S., Masato, G., Milton, S. F., Roberts, M. J., Rowell, D. P., Sanchez, C., Shelly, A., Sinha, B., … Xavier, P. K. (2015). The Met Office Global Coupled model 2.0 (GC2) configuration. *Geoscientific Model Development*, *8*(5), 1509–1524. https://doi.org/10.5194/gmd-8-1509-2015

Xie, S. P., Annamalai, H., Schott, F. A., & McCreary, J. P. (2002). Structure and mechanisms of South Indian Ocean climate variability. *Journal of Climate*, *15*(8). https://doi.org/10.1175/1520-0442(2002)015<0864:SAMOSI>2.0.CO;2

Yang, J., Liu, Q., Xie, S. P., Liu, Z., & Wu, L. (2007). Impact of the Indian Ocean SST basin mode on the Asian summer monsoon. *Geophysical Research Letters*, *34*(2). https://doi.org/10.1029/2006GL028571

Yokoi, S., Takayabu, Y. N., & Chan, J. C. L. (2009). Tropical cyclone genesis frequency over the western North Pacific simulated in medium-resolution coupled general circulation models. *Climate Dynamics*, *33*(5). https://doi.org/10.1007/s00382-009-0593-9

Yokoi, T., Tozuka, T., & Yamagata, T. (2008). Seasonal variation of the Seychelles Dome. *Journal of Climate*, *21*(15). https://doi.org/10.1175/2008JCLI1957.1

Yu, L. (2003). Variability of the depth of the 20°C isotherm along 6°N in the Bay of Bengal: Its response to remote and local forcing and its relation to satellite SSH variability. *Deep-Sea Research Part II: Topical Studies in Oceanography*, *50*(12–13). https://doi.org/10.1016/S0967-0645(03)00057-2